Effects of deposition dynamics on epitaxial growth

2007 J. Phys.: Condens. Matter 19 486001

(http://iopscience.iop.org/0953-8984/19/48/486001)

IOP PUBLISHING JOURNAL OF PHYSICS: CONDENSED MATTER

J. Phys.: Condens. Matter **19** (2007) 486001 (13pp) doi:10.1088/0953-8984/19/48/486001

Effects of deposition dynamics on epitaxial growth

Jikeun Seo[1], Hye-Young Kim[2] and J-S Kim[3]

[1] Department of Ophthalmic Optics, Chodang University, Muan 534-701, Korea
[2] Department of Physics, The Pennsylvania State University, University Park, PA 16802, USA
[3] Department of Physics, Sook-Myung Women's University, Seoul 140-742, Republic of Korea

Received 30 August 2007, in final form 4 October 2007
Published 5 November 2007
Online at stacks.iop.org/JPhysCM/19/486001

Abstract

Dynamic effects, such as steering and screening during deposition, on epitaxial growth (Cu/Cu(001)) were studied by kinetic Monte Carlo simulations that incorporate molecular dynamics simulations to account for the interaction between the deposited and substrate atoms. Three characteristics of the surface morphology with grazing angle deposition were noted: enhanced surface roughness, an asymmetric mound, and asymmetric slopes of the mound sides. Regarding their dependence on both deposition angle and substrate temperature, reasonable agreement was found between the simulation and previous experimental results. The growth characteristics of grazing angle deposition were mainly caused by inhomogeneous distribution of deposition flux due to the steering and screening effects, with the steering effects playing the dominant role. It was also noted in the present simulation that each side of a mound was composed of various local facets instead of a selected facet. Thus, slope selection does not necessarily signify facet selection.

1. Introduction

For the tailored growth of a structure on a substrate both energetic parameters, such as surface and interface energies, and kinetic parameters, such as diffusion barriers, have been considered. However, the variables related to the dynamics of the deposited atoms, other than the deposition flux, have not been seriously considered. Using spot profile analysis of low energy electron diffraction (SPA-LEED), Dijken *et al* [1] recently observed that the Cu islands formed on Cu(001) displayed rectangular symmetry, as opposed to the square symmetry of the substrate when a 0.5 monolayer (ML) of Cu was deposited at a deposition angle (θ) of 80° from the surface normal. They suggested a model in which the interaction between the deposited and substrate atoms directs the deposited atom—the so-called steering effect—resulting in an inhomogeneous deposition flux that in turn forms rectangular islands.

In our previous study [2], kinetic Monte Carlo (KMC) simulations in conjunction with molecular dynamics (MD) simulation of the deposited atoms confirmed this hypothetical model

in the submonolayer regime. Since steering effects are unavoidable during deposition, they affect thin film growth to some degree, even for normal deposition [3, 4] and for different substrates such as Ag(110) [5]. It has been also shown that deposition dynamics are a cause of unstable growth of thin films on a vicinal surface [6]. These studies have demonstrated that the dynamic parameters involved in the deposition process, which have been largely ignored in previous studies, exert a considerable influence on thin film growth. The instability induced by steering effects was also theoretically predicted by Raible *et al* [7].

Dijken *et al* [8] observed that, in the growth of a thicker film (40 ML) with $\theta = 80°$, the surface is much rougher than that at $\theta = 0°$. It has also been observed that the slope of the mound facing the deposition direction is much steeper than on the side shadowed from deposition [8]. Although a qualitative model has been suggested to relate the experimental results to the inhomogeneous deposition flux due to the steering and screening effects [9], few corroborative simulation studies have been conducted.

In the present study, kinetic Monte Carlo (KMC) simulations were performed in conjunction with MD simulations to investigate the effects of the dynamic processes on the growth of thin films beyond the submonolayer regime. The principal results are as follows. Roughness increased substantially with increasing deposition angle. The mound formed during thick film growth had, for the most part, rectangular symmetry with sides elongated in the direction perpendicular to the deposition direction. (Some exceptions, such as the formation of square mounds and ripple structure, will also be discussed.) The slopes of the illuminated and shadowed sides of the mound differed significantly, which is consistent with the experimental results [8]. These three characteristic morphological features are attributable to inhomogeneous distribution of deposition flux due mainly to steering rather than screening effects. In addition, we found that each side of a mound was formed of various local facets instead of a selected facet, and the observed dependence of (mean) mound slope on growth conditions is due to variations in the relative population of the local facets.

2. Simulation schemes

A KMC simulation was utilized to study thin film growth by deposition. In most of the previous KMC simulations the deposition process involved randomly positioning atoms at arbitrary adsorption sites. In the present study, however, if the deposition process was selected via normal KMC simulation, then a MD routine was applied to simulate the trajectory of a deposited atom, which was determined by the interaction between the deposited and substrate atoms [10].

Details of the simulation are as follows. The Cu(001) substrate lies on the xy-plane (at $z = 0$) with the x-axis lying parallel to the [110] direction. In the process, deposition begins at a height of $11a_z$ above the highest position of the growing film and deposited atoms are incident along the x-axis. Here, a_z is the interlayer spacing of Cu(001).

The interaction between a deposited atom and substrate atoms is calculated by summing pairwise Lennard-Jones potentials: $U(r) = 4D[(\sigma/r)^{12} - (\sigma/r)^6]$, where $D = 0.4093$ eV, $\sigma = 2.338$ Å, [11] and r is the distance between two atoms. The initial kinetic energy of the deposited atom is set to 0.15 eV, which corresponds to the melting temperature of copper. During each deposition step, all substrate atoms are assumed to be frozen in their positions. During each deposition, the incident atom approaches the substrate as dictated by MD and stops just before it feels the repulsive force from the substrate atoms. The distance from the terminal position to the encountering substrate atom is usually around $0.9\,a_{\mathrm{nn}}$ (a_{nn} is the nearest neighbour distance). Then, the atom is positioned from the terminal position to the nearest four-fold hollow site, since epitaxial (pseudo-morphic) growth is observed experimentally on Cu(001) [1].

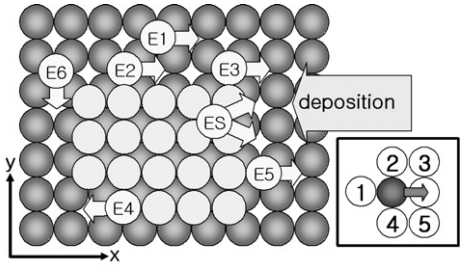

Figure 1. Diffusion processes considered in the simulation. Inset: neighbouring atoms of a moving atom considered in the simulation.

Table 1. Diffusion barriers and parameters adopted in our simulation. The same notation is used for each diffusion process as in figure 1.

Type of diffusion	Diffusion barrier
E1	0.42 eV
E2	0.36 eV
E3	0.46 eV
E4	0.62 eV
E5	0.68 eV
E6	0.18 eV
ES barrier (ES)	0.07 eV (0.42 + 0.07 eV)
ES barrier (kink site)	0.035 eV
Jump frequency (ν_0)	3.6×10^{12}
Deposition rate (F_0)	0.25 ML min^{-1}

For an atom depositing near the step edge, four-fold hollow sites defined by at least two atoms forming the step edge were allowed for adsorption, but the atom was then funnelled down to a four-fold hollow site in the lower terrace [12]. Although transient mobility of deposited atom may affect uphill (vice versa downhill) flux near step edge [13], such effects are not taken into account in the present simulation. For all simulations, a deposition rate of 0.25 ML min^{-1}, the experimental one of Dijken *et al* [1], was used.

Between two sequential deposition processes, a KMC simulation was performed to simulate the diffusion of atoms on the substrate. In the KMC simulation, only diffusion into empty fcc lattice sites is allowed; no exchange diffusion is permitted [14]. The simulated system is composed of 400×400 atomic lattice sites on the fcc(001) surface.

We used 32 different barriers corresponding to the 2^5 configurations determined by the existence or absence of atoms in the five sites around a moving atom, as depicted in the inset of figure 1. The barriers were divided into six groups according to their magnitude to reduce computing time; barrier values were adopted from Furman and co-workers [15, 16]. In addition to these six barrier values, five barriers accompanying the Ehrlich–Schwoebel barrier were also considered. The step Ehrlich–Schwoebel (ES) and the kink ES barrier were 0.07 and 0.035 eV, respectively. The principal diffusion processes are depicted in figure 1 and their barrier values listed in table 1.

Note that the barrier (E2) for diffusion along the step edge was set at 0.36 eV in the present simulation to save computation time. Although no consensus exists on the value of the E2 barrier, the employed value is larger than the reported values of 0.2–0.3 eV [14, 16]. We investigated the dependence of surface morphology, roughness (figure 2(a)) and mean

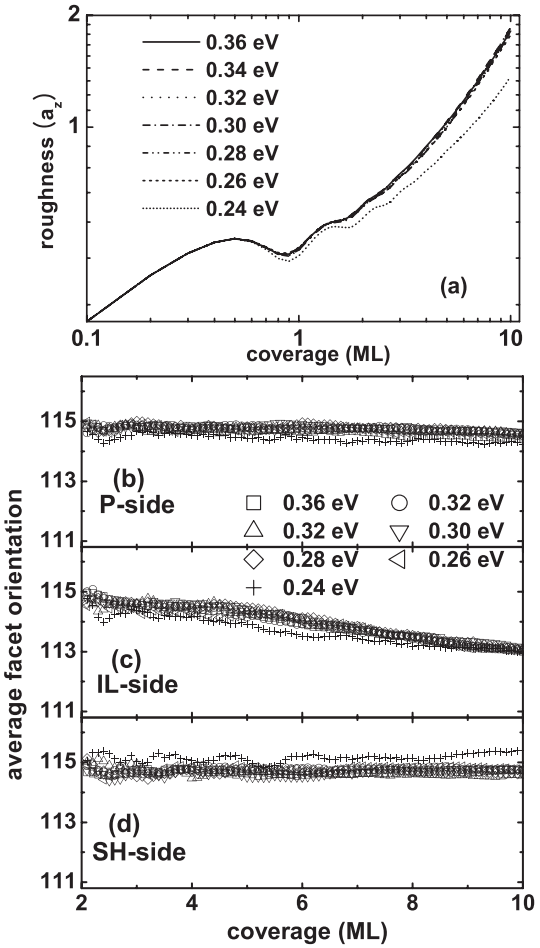

Figure 2. Roughness and the mean slopes of three sides of the mound versus coverage for various E2 barriers. (a) Roughness and the mean mound slopes of (b) P-side, i.e. two sides of the mound perpendicular to the deposition direction, (c) IL-side, i.e. the side facing the deposition direction, and (d) SH-side, i.e. the shadowed (or back) side of the mound in the deposition direction. The deposition angle is 80° at $T = 250$ K.

mound slope (figures 2((b)–(d))) on E2. Morphology showed no noticeable dependence on E2 down to 0.26 eV; however, for E2 = 0.24 eV, roughness decreased significantly and the slope differed from that obtained at higher E2 values. In our simulation with E2 = 0.36 eV, most experimentally observed features were well reproduced. Hence, the E2 does not seem that much smaller, even if it is the case, than at 0.26 eV.

The surface roughness was determined by the root-mean-square fluctuation in surface height around the mean height. The mound radius was determined by the first zero of the height–height correlation function $G(\vec{r}) = \langle h(\vec{r})h(0)\rangle - \langle h(0)\rangle^2$. All presented results were obtained from the average of 20 simulations under identical conditions. Unless otherwise noted, the distance in a plane is in units of the nearest-neighbour distance $a_{\rm nn}$ and the distance in the vertical direction is in units of a_z. Here, $a_{\rm nn}$ is $a/\sqrt{2}$ and the interlayer distance is $a_z = a/2$, where a is the lattice constant of Cu.

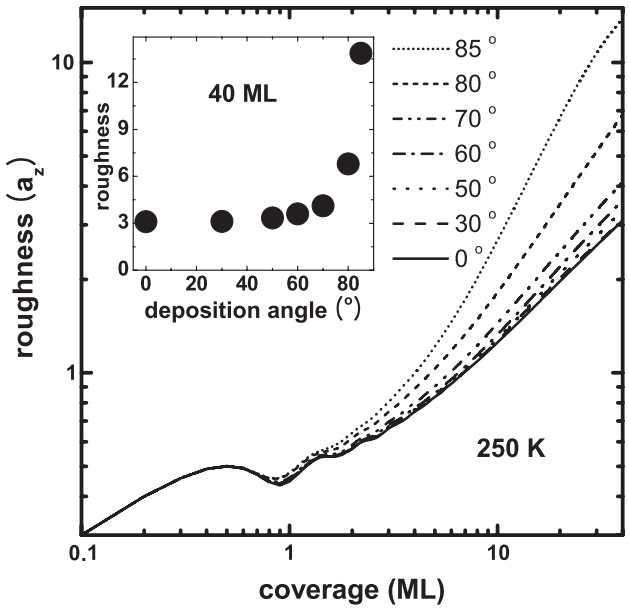

Figure 3. Surface roughness as a function of coverage and deposition angle. Substrate temperature: 250 K. Inset: roughness as a function of the deposition angle at a coverage of 40 ML. The error bar for each data point is located within each symbol.

3. Results

3.1. Roughness

Figure 3 shows surface roughness as a function of coverage (Θ), when Cu atoms are deposited at various deposition angles on Cu(001) at 250 K. The most notable feature is that, at the same coverage, the surface becomes rougher as the deposition angle increases, as also observed experimentally [8]. As Θ increases, the difference in roughness between deposition at the grazing angle and normal deposition ($\theta = 0°$) increases. At $\Theta = 40$ MLs, the roughness with $\theta = 85°$ is about four times greater than normal deposition (inset of figure 3).

3.2. Mound radius

Figure 4 shows the mound radius of a 40 ML thick Cu film grown on Cu(001) at 250 K under the same growth conditions described by Dijken *et al* [1, 8] as a function of θ. When atoms are deposited in the normal direction ($\theta = 0°$), square mounds are formed with the same four-fold symmetry as the substrate (in this case, the open and solid symbols overlap in figure 4). However, as θ increased, the aspect ratio of the rectangular mounds also increased, with elongated sides along the y-axis and reaching a maximum at $\theta = 80°$ (the x- and y-axes are defined in figure 1). In contrast, at $\theta = 85°$, the aspect ratio decreased back to approximately 1.

Dijken *et al* [8] reported a ripple-like structure at $\theta = 80°$ for $\Theta = 40$ ML, and re-entrant behaviour from the ripple-like structure to a mound structure was observed at $\theta = 85°$. In the present simulation, a similar re-entrant behaviour from a rectangular to a square mound structure as θ increased from 80° to 85° was also observed, although the rectangular mounds did not fully develop into ripple-like structures at $\theta = 80°$.

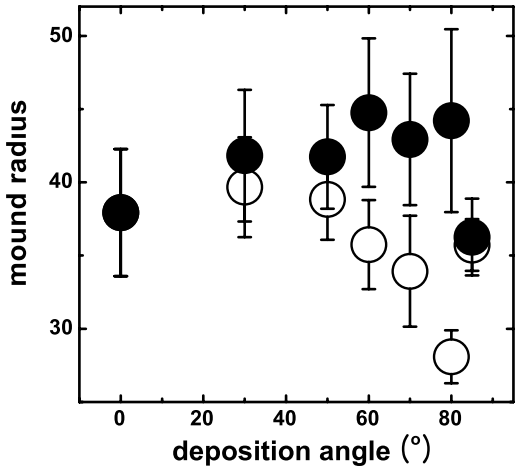

Figure 4. Mound radius as a function of the deposition angle at a coverage of 40 ML. Substrate temperature 250 K. Open and solid circles signify the radii along the x- and y-axes, respectively.

3.3. Mound slope

To characterize the mean slopes of the mounds, we investigated the local slope at each step on each side of the mound, defined as the step height divided by the width of the adjacent lower terrace. Most steps on the sides of the mounds are one atomic layer in height. Thus, if the width of a lower terrace adjacent to a step is 0.5 a_{nn}, then the local slope is $a_z/0.5\ a_{\mathrm{nn}}$, which corresponds to the slope of the {1, 1, 1}-facet on the fcc(001) surface. For steps with terrace widths of 1.5 and 2.5a_{nn}, the corresponding local slopes are those of the {1, 1, 3}- and {1, 1, 5}-facets, respectively. Hereafter, the step-terrace structure with a local slope of the {1, 1, j} facet will be referred to as the *local*{1, 1, j}*-facet*.

In our simulation, we found that various types of local facets coexist on each side of the mound. Figure 5 shows the distribution of the local facets as a function of coverage for thin films grown by deposition at $\theta = 0°$ and a substrate temperature (T) of 250 K. The mean slope increased with increasing Θ (inset of figure 5; note that the {1, 1, 1}-facet is the steepest). At $\Theta = 100$ ML, the mean terrace width reached 2.13a_{nn}, close to that of the {1, 1, 5}-facet; however, the relative population of the local {1, 1, j}-facet was 11% ($j = 1$), 43% ($j = 3$), 27% ($j = 5$), 13% ($j = 7$) and 7% ($j = 9$) at this coverage (the proportion of local facets with slopes less than that of the {1, 1, 11}-facet was negligible). Therefore, even though the mean slope of the sides converges to that of the {1, 1, 5}-facet, the actual relative population of local {1, 1, 5}-facets was only 27% and the rest of the sides were composed of different local facets with various local slopes.

Figure 6 shows the distribution of local facets on each side of the mounds (IL, illuminated; SH, shadowed; P, perpendicular) after depositing 40 ML at 250 K and at various deposition angles. Distributions of the local facets were similar for the three sides of the mounds for $\theta < 50°$; however, the distributions varied as the deposition angle increased. For $\Theta = 40$ ML and $\theta = 80°$, 77% of the IL-sides were composed of local {1, 1, 1}-facets, but only 23% of the SH-side was made up of local {1, 1, 1}-facets; thus, its mean slope was less steep than that of the IL-side.

Dijken *et al* [8] investigated the mean slopes of the sides of a mound formed during the growth of a 40 ML thick Cu film on Cu(001) at 250 K using SPA-LEED with varying deposition angles. Figure 7 compares the experimental results with our simulation, i.e. mean

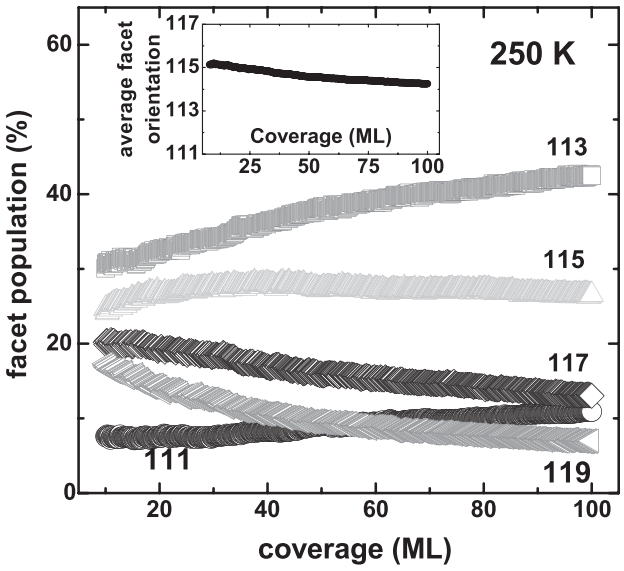

Figure 5. Relative population of local facets that make up the sides of the mounds formed by normal deposition ($\theta = 0°$) at 250 K. Inset: average slope of the mounds as a function of coverage.

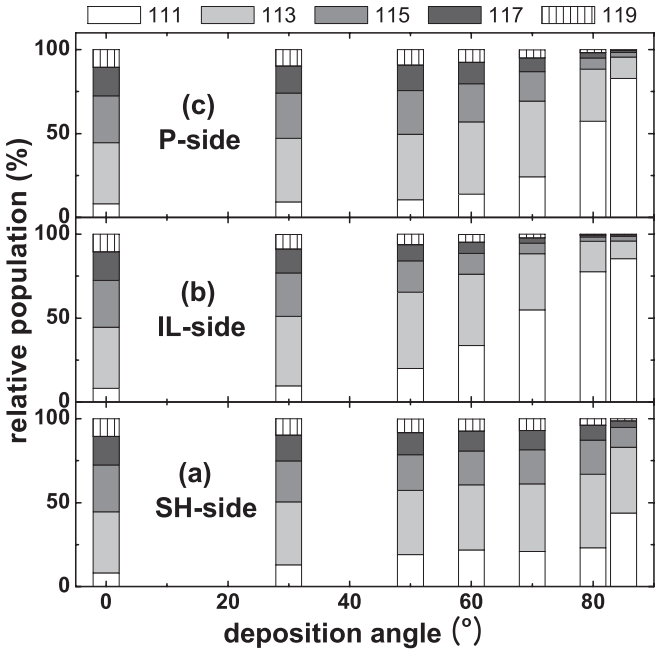

Figure 6. Relative population of local facets that make up the sides of the mounds formed by depositing 40 ML at 250 K and at various deposition angles. (a) P-side: two sides of a mound perpendicular to the deposition direction. (b) IL-side: the side facing the deposition direction. (c) SH-side: the shadowed (or back) side of the mound in the deposition direction.

facet orientation. The simulation reproduced the experimental results for all three sides of the mound reasonably well.

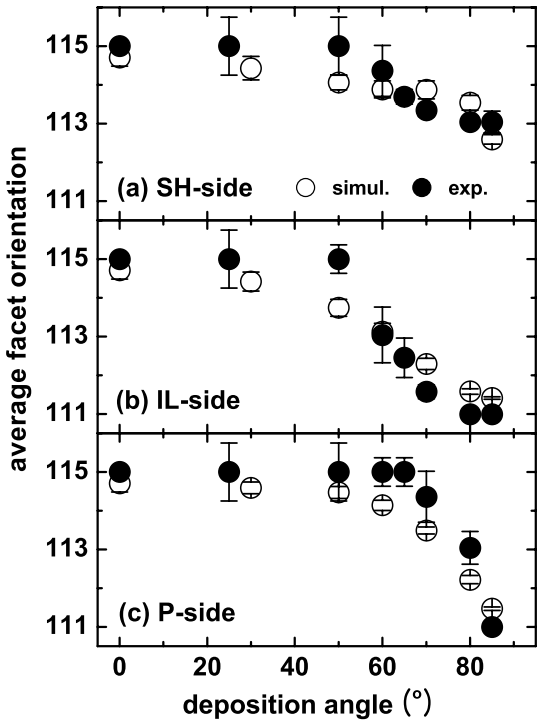

Figure 7. Average facet orientation of mounds for a 40 ML thick Cu film grown on Cu(001) at 250 K as a function of θ for the (a) SH-, (b) IL- and (c) P-sides of the mounds. Filled and open symbols denote experimental [8] and present simulation results, respectively.

4. Discussion

4.1. Inhomogeneous deposition flux

In the previous section, we noted that film roughness and mound shape are dependent on dynamic variables, such as the deposition angle. Such angular dependence can be attributed to deposition dynamics, including the steering of the trajectory of the deposited atom due to its interaction with substrate atoms and the screening effects of the deposited atoms due to the geometrical structure of the substrate. Both effects cause inhomogeneous distribution of deposition flux, making the growth of thin films sensitive to deposition conditions.

The deposition flux distribution was investigated by a MD simulation on an eight-layer-high mound of 60×60 base area, surrounded by $\{1, 1, 5\}$-facets. Figure 8(a) shows the deposition flux over the mound in a grey scale for $\theta = 80°$. Figure 8(b) shows the deposition flux along a line passing through the centre of the mound along the x-axis. It shows strong asymmetry, that is, the deposition flux on the IL-side is two to four times larger than the average deposition flux, while that on the SH-side is only 10–50% of the average. In particular, the enhancement of the flux near the IL-side edge of the top terrace is pronounced. The simulation with the mounds surrounded by the different facets showed the same trend, i.e. enhanced deposition flux on the IL-side and reduced deposition flux on the SH-side.

Such inhomogeneous distribution of deposition flux gives rise to different growth rates on either side; thus, the film is rougher than the film grown under normal deposition conditions (figure 3). In particular, the enhanced deposition flux near the front edge of the top terrace

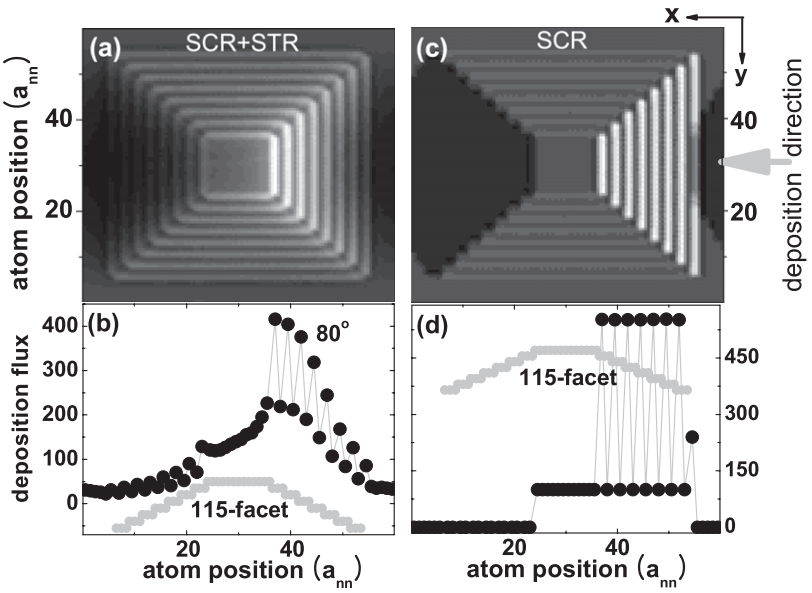

Figure 8. Deposition flux distribution calculated by a MD simulation. Atoms were deposited at a grazing angle of 80° on an eight-layer-high mound surrounded by (1, 1, 5)-facets with reference to (a), (b) both the steering and screening effect, and (c), (d) the screening effect only. (a), (c) The deposition flux distribution is shown as a grey scale, where a brighter tone indicates a higher flux. (b), (d) Deposition flux distribution on a line through the centre of the mound along the *x*-axis. The ordinate is the percentage deposition flux relative to the average deposition flux. The mound is depicted as grey circles.

increased the destabilizing current biased by the ES barrier and significantly roughened the surface. (See the discussion in the following subsection for further details.)

The asymmetric slopes of the mounds observed for $\theta > 50°$ (figure 6) can also be explained by inhomogeneous distribution of deposition flux in the following terms. First, the higher deposition flux on the IL-side compared to the SH-side is equivalent to a growth environment with a lower growth temperature on the IL-side than on the SH-side. Thus, the terrace size on the IL-side is narrower than that on the SH-side, or equivalently, the slope on the IL-side is steeper than that on the SH-side, as observed in a previous experiment [8].

In addition, the flux distribution on the top terrace strengthened asymmetric slope formation. Figure 8(b) shows that the deposition flux near the edge toward the IL-side is much higher than that near the opposite edge, which resulted in an increased density of islands on the top terrace near the edge of the IL-side. The sequential formation of islands on the top terrace, preferentially close to the edge, makes mounds having steps with a narrower terrace width or steeper slope on the IL-side than on the SH-side.

4.2. Steering versus screening effects

As a film becomes thicker, in addition to the steering effects the geometric screening effects also play an important role. To study the contribution of the individual dynamic effect on thin film growth, another set of growth simulations was performed, taking only the geometric screening effects into account. In this simulation, the trajectory of the deposited atom is a straight line, determined by the initial position and velocity of the atom. All other growth conditions are as outlined in previous subsections.

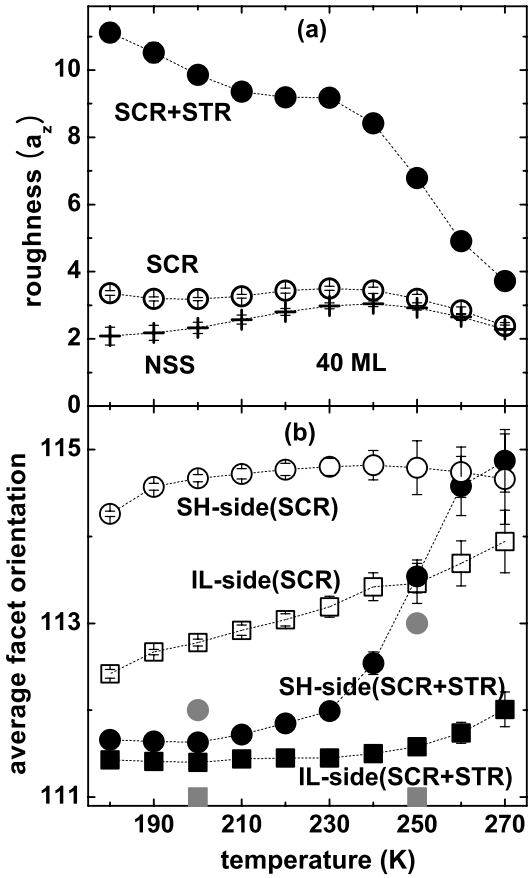

Figure 9. Simulation results with $\theta = 80°$ and $\Theta = 40$ ML. (a) Roughness as a function of temperature for (+) random deposition (NSS), (open circles) deposition with screening effects alone (SCR) and (solid circles) deposition with both screening and steering effects (SCR + STR). (b) Average facet orientation for the SH-side (circle) and the IL-side (square). Open (solid) symbols for SCR (SCR + STR). Solid and grey circle (square) is an experimental values for the SH(IL)-side. Under some experimental conditions, when two facets were observed, the plotted one is the mean of the two.

Figure 9(a) shows roughness evolution as a function of temperature for three different cases: assuming no steering and screening effects (NSS) or random deposition, with geometric screening effects only (SCR) and normal simulation taking all dynamic effects, that is, both steering and screening effects (SCR + STR), into consideration. When the dynamic effects were not taken into account (NSS), then roughness displayed a bell-shaped temperature dependence. However, when the screening effects were included, the roughness of the film increased slightly as the substrate temperature decreased below ∼200 K. In sharp contrast, the roughness was dramatically enhanced if the steering effects were included. This indicates that the steering rather than the screening effects plays a dominant role in the growth of thin films.

The origin of the difference in the roughness between the two cases, SCR and SCR + STR, lies in their different flux distributions, as shown in figure 8. The most notable difference was found in the flux on the top terrace. In figures 8(a) and (b), the flux distribution for SCR + STR showed clear flux enhancement near the front edge of the top terrace, as well as on the IL-side.

No such enhancement of flux on the top terrace was found for SCR, as shown in figures 8(c) and (d). The steering effects induced a vertical flux redistribution in addition to the lateral redistribution. Thus, the relaxation of the steering effects should be less efficient than that of the screening effects because the former is achieved by inefficient interlayer diffusion over the ES barrier, while the latter occurs via relatively efficient in-plane diffusion. Therefore, the increased atom density on the top layer accelerated the roughening of the film, which differed from the SCR case.

In figure 9(b), the mean slopes for the IL- and SH-sides are shown as a function of growth temperature for both SCR and SCR + STR. The mean slopes of both sides are steeper for SCR + STR than for SCR. In addition, the temperature dependence of the mean slopes differed for the two cases. For SCR, the difference in the mean slope between the IL- and SH-sides decreased with increasing temperature. In contrast, for SCR + STR, the difference in the mean slopes increased with temperature. Compared to the experimental results in figure 9(b), we found that the average facet orientations for SCR + STR reproduced the experimental values better than those for SCR. This observation also indicated that the steering effects steepened the slopes and played a major role in shaping the mounds.

In short, for thin film growth at the grazing deposition angle, enhanced surface roughness and the difference in slope between the IL- and SH-sides of mounds resulted mainly from steering rather than screening effects (figure 9). Noting that the main difference between steering and screening effects is enhanced deposition flux near the front edge of the top terrace, the observed characteristics of films grown at the grazing deposition angle are largely determined by the growth characteristics of the top layer as the growth front.

4.3. Ripple-like structure

Dijken *et al* reported that the mound structure is maintained for $\theta < 70^\circ$ during the growth of 40 ML of Cu on Cu(001) at 250 K. When θ reached 80°, the mound structure was transformed into a ripple structure along the y-direction. When θ reached 85°, however, the mound structure recovered. As shown in figure 4, the present simulation reproduced similar results. For SCR + STR at 250 K, we observe an increase in the aspect ratio with the long side along the y-axis as θ approached 80° and then the decrease of the aspect ratio at $\theta = 85^\circ$ (figure 4). However, even at $\theta = 80^\circ$ where the aspect ratio is maximum, the mound structure was still retained, since the zero of $G(\vec{r})$ or the mound radius is well-defined in both directions (figure 10(a)). This is not in agreement with the experimental result. Only if the simulation temperature is lowered below 220 K is a ripple structure is found upon deposition of a 40 ML film at $\theta = 80^\circ$, judging from the absence of zero of $G(\vec{r})$ (figure 10(b)).

Shim and Amar [17] reproduced the ripple structure with a simulation that considered screening effects only. We reproduced most of their results only by considering screening effects. However, the ripple-like structure was observed only at a substrate temperature below 220 K.[4] The substrate temperature affects not only the diffusion kinetics but also deposition flux distribution via the shape and density of the mounds. Hence, it is not clear yet what the most relevant process for the growth of the ripple structure is.

5. Summary and conclusion

We performed a hybrid simulation incorporating MD and KMC simulations to study thin film growth by grazing angle deposition. We observed a notable increase in surface roughness

[4] Since the deposition temperature is not given and the growth condition is not clearly described in the paper of Shim and Amar [17], no comparison with their results is allowed.

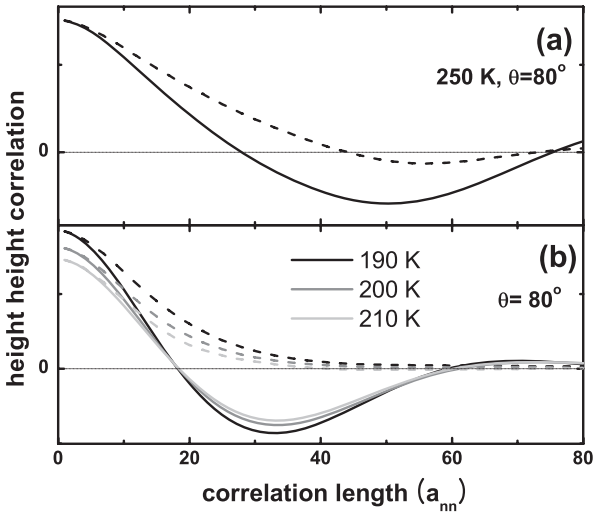

Figure 10. Height–height correlation function at a coverage of 40 ML: (a) $T = 250$ K and $\theta = 80°$; (b) $T < 220$ K and $\theta = 80°$. Continuous (dashed) line denotes the correlation function along the x- (y-)axis.

and asymmetry in both mound shape and slope compared to thin film growth via normal deposition. The results were in good agreement with previous experimental observations [8], even semi-quantitatively. The present simulation, although based on a simple premise, appears to reflect the most critical characteristics of the deposition process in relation to thin film growth. The ripple-like structure is, however, not reproduced in the present simulation under the experimental condition. Further works from both experimental and theoretical sides are required to resolve the discrepancy[5].

We found that the structural features of the films grown by grazing angle deposition are mainly attributable to steering rather than screening effects. In particular, the inhomogeneous deposition flux on the top terrace, induced by the steering effects, is the most influential factor.

An additional interesting observation is that the sides of a mound are not composed of a selected facet. Instead, a variety of local facets coexist and the selected mound slope observed experimentally represents their mean slope only. Therefore, slope selection does not necessarily signify facet selection.

Acknowledgment

This study was supported by the Korea Science and Engineering Foundation (M10503000210-06M0300-21010).

References

[1] Dijken S V, Jorritsma L C and Poelsema B 1999 *Phys. Rev. Lett.* **82** 4038
[2] Seo J, Kwon S-M, Kim H-Y and Kim J-S 2003 *Phys. Rev.* B **67** R121402
[3] Montalenti F, Sorensen M R and Voter A F 2001 *Phys. Rev. Lett.* **87** 126101

[5] Recently, Wormeester *et al* have re-investigated the system, now by applying a scanning tunnelling microscope (STM) as well as SPA-LEED, because a diffraction profile could be interpreted in several different ways [18]. The most important observation is that a strongly elongated mound structure rather than a ripple structure is formed.

[4] Montalenti F and Voter A F 2001 *Phys. Rev.* B **64** R081401
[5] Ceriotti M, Ferrando R and Montalenti F 2006 *Nanotechnology* **17** 3556
[6] Seo J, Kim H-Y and Kim J-S 2005 *Phys. Rev.* B **71** 075414
[7] Raible M, Linz S J and Hänggi P 2000 *Phys. Rev.* E **62** 1691
[8] Dijken S V, Jorritsma L C and Poelsema B 2000 *Phys. Rev.* B **61** 14047
[9] Wormeester H and Poelsema B 2002 *Phys. Rev.* B **66** 165406
[10] A similar approach has been undertaken in the following studies: Jacobsen J, Cooper B H and Sethna J P 1998 *Phys. Rev.* B **58** 15847
Levine S W, Engstrom J R and Clancy P 1998 *Surf. Sci.* **401** 112
[11] Sanders D E and DePristo A E 1991 *Surf. Sci.* **254** 341
Sanders D E, Halstead D M and DePristo A E 1992 *J. Vac. Sci. Technol.* A **10** 1986
[12] Amar J G and Family F 1996 *Phys. Rev.* B **54** 14742
[13] Yu J and Amar J G 2002 *Phys. Rev. Lett.* **89** 286103
[14] Montalenti F and Ferrando R 1999 *Phys. Rev.* B **59** 5881 and references therein
[15] Furman I, Biham O, Zuo J-K, Swan A K and Wendelken J F 2000 *Phys. Rev.* B **62** R10649
[16] Mehl H, Biham O, Furman I and Karimi M 1999 *Phys. Rev.* B **60** 2106
[17] Shim Y and Amar J G 2006 *Phys. Rev. Lett.* **98** 046103
[18] Wormeester H, Rabbering F, Stoian G, van Gastel R and Poelsema B, unpublished